Int. J. Impact Engng Vol.14, pp.95–106, 1993
Printed in Great Britain

0734-743X/93 $6.00+0.00
Pergamon Press Ltd

HYPERVELOCITY TESTING OF ADVANCED SHIELDING CONCEPTS FOR SPACECRAFT AGAINST IMPACTS TO 10 KM/S

M. B. BOSLOUGH*, J. A. ANG*, L. C. CHHABILDAS*, W. D. REINHART*, C. A. HALL*
B. G. COUR-PALAIS**, E. L. CHRISTIANSEN*** and J. L. CREWS***

*Sandia National Laboratories, Albuquerque, New Mexico 87185
**McDonnell Douglas Space Systems Division, Houston, Texas 77062
***NASA, Johnson Space Center, Houston, Texas 77058

ABSTRACT

Experiments have been performed on NASA state-of-the-art hypervelocity impact shields using the Sandia Hypervelocity Launcher (HVL) to obtain test velocities greater than those achievable using conventional two stage light-gas gun technology. The objective of the tests was to provide the first experimental data on the advanced shielding concepts for evaluation of the analytical equations (shield performance predictors) at velocities previously unattainable in the laboratory, and for comparison to single Whipple Bumper Shields (WBS) under similar loading conditions. The results indicate that significantly more mass is required on the back sheet of the WBS to stop an approximately flat-plate particle impacting at 7 km/sec and at 10 km/sec than the analytical equations (derived from spherical particle impact data) predicted. The Multi-Shock Shield (MSS) consists of four ceramic fabric bumpers, and is lighter in terms of areal density by up to 33%, but is as effective as the heavier WBS under similar impact conditions at about 10 km/s. The Mesh Double Bumper shield (MDB) consists of an aluminum wire mesh bumper, followed by a sheet of solid aluminum and a layer of Kevlar® fabric. It provides a weight savings in terms of areal density of up to 35% compared to the WBS for impacts of around 10 km/s.

1. INTRODUCTION

There is an increasing requirement to protect spacecraft from the serious threat posed by naturally occurring meteoroids and human-generated orbital debris in low earth orbit. The meteoroid threat is primarily dust size particles having an average relative impact velocity of 20 km/sec; for very large, long-duration spacecraft, the probability of an impact by a larger particle of human-generated debris becomes significant. The orbital debris size distribution of this "space junk" ranges from micron size flakes of paint to inactive satellites (Kessler *et al.*, 1989). The most probable size of impacting particles for spacecraft such as the Space Station Freedom is expected to be in the millimeter to centimeter range. The practicable passive shielding capability for such a spacecraft will defend against a particle up to a few centimeters in diameter with an average relative impact velocity of 10 km/sec. Other schemes such as avoidance maneuvering will need to be implemented for the larger debris that can be tracked by radar and other means (Interagency Group, 1989).

The need for low-weight passive hypervelocity impact shielding is obvious, and NASA has been instrumental in the area of spacecraft hypervelocity shielding research. Several innovative low-weight shielding concepts have been developed by NASA including the Multi-Shock Shield (Cour-Palais and Crews, 1990) and the Mesh Double Bumper (Christiansen, 1990). The velocity limitations of existing two stage light-gas guns resulted in a research project using the Sandia Hypervelocity Launcher (Chhabildas *et al.*, 1992a, b) to attain even higher impact test velocities to characterize these new shields. This paper will discuss the results of these experiments.

2. DEBRIS SHIELD DESIGNS

2.1 Whipple Bumper Shield (WBS)

The conventional shield that has been used to protect satellite systems from hypervelocity meteoroid impact is called the Whipple Bumper Shield (Whipple, 1947). The effectiveness of this shield comes from its ability to fragment the impacting object into a debris cloud which is solid, liquid, and/or vapor, depending on the impact velocity. The WBS typically consists of a single sheet of aluminum, called the bumper, which provides a surface away from the hull of the spacecraft on which an incoming particle of debris can impact. By the time the resulting debris cloud reaches the spacecraft, it will disperse and the kinetic energy density will decrease. In the present study, the Whipple shield design consists of two spaced aluminum sheets: an aluminum bumper sheet separated from an aluminum "back" sheet. For the present investigation, the back sheet is intended to be an element of the shield rather than a hull plate bulkhead or a pressure vessel wall. Two thicknesses of bumpers were tested in this study: 1) 0.30 mm thick 2024-T3 aluminum, and 2) 1.27 mm thick 6061-T6 aluminum. In all cases, the bumper was placed 305 mm in front of the back sheet. The results of a few WBS tests have already been published (Ang *et al.*, 1992; Chhabildas *et al.*, 1992c; Hertel *et al.*, 1992). Some of these results are summarized here, providing a baseline for comparison to the more advanced shielding concepts.

2.2 Multi-Shock Shield (MSS)

The Multi-Shock Shield concept (Cour-Palais and Crews, 1990), is based on the use of a number of spaced bumpers placed in front of a back sheet element to excite the projectile impact debris to higher internal energy states (and temperatures) by repeated collisions. The final state of the projectile and shield material impacting the back sheet depends on the initial impact velocity, the mass density of the first bumper, the number of subsequent bumpers and their mass densities, and the spacing between the individual bumpers and the back sheet. An optimally designed MSS could result in a significant weight saving over the conventional WBS, primarily because the back sheet will be much lighter. The MSS used in these tests had four Nextel® BF54 or AF62 ceramic fabric bumpers (Fig. 1a) spaced 76.2 mm apart, with an aluminum alloy back sheet the same distance behind the last bumper. Nextel® is the trade name for the high-temperature, ceramic fabrics made by the 3M company. BF54 is woven from fibers composed of 70% aluminum oxide, 28% silicon dioxide and 2% boric oxide and has an areal density of 0.108 g/cm^2. AF62, on the other hand, has the same weave but the fiber composition is 62% aluminum oxide, 24% silicon dioxide and 14% boric oxide, which makes it lighter at 0.100 g/cm^2. The back sheet was 6061-T6 aluminum with a thickness of 2.03 mm.

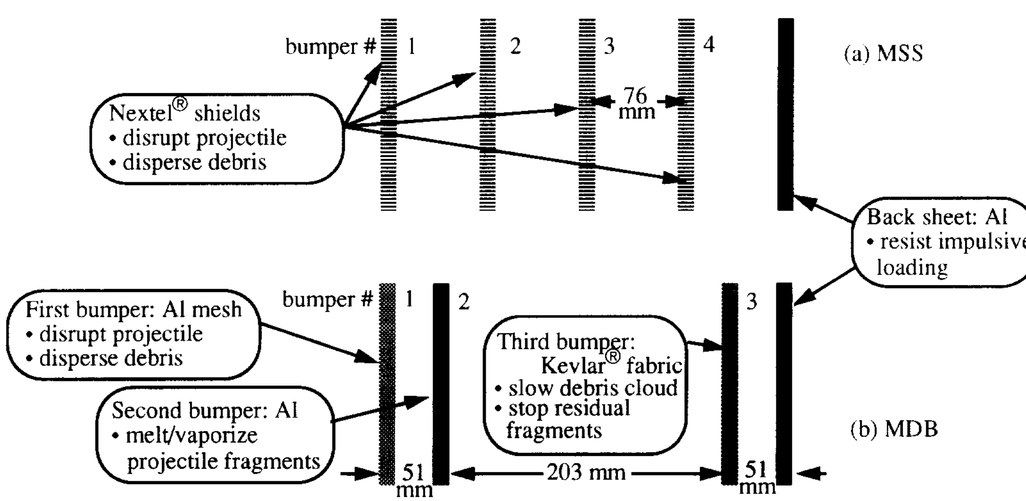

Fig. 1. Advanced Debris shielding concepts: (a) Multi-Shock Shield, (b) Mesh Double Bumper.

2.3 Mesh Double Bumper Shield (MDB)

The Mesh Double Bumper shield (Christiansen, 1990) provides weight savings of approximately 50% at two-stage light-gas gun velocities for a sphere compared with conventional dual-sheet aluminum WBS's. The MDB shield is based on the concept of a dual bumper system with an initial mesh bumper that disrupts the projectile, followed by a high strength fabric layer that slows the expansion of the debris cloud prior to contacting the back sheet (Fig. 1b). The mesh is composed of overlapping wires in a square pattern. Where the wires overlap, localized mesh areas with greater bumper thickness are created which contribute to the disruptive forces exerted on the projectile by increasing the shock duration in the projectile during the impact event. Generally, in two stage light-gas gun testing with projectile diameters of around 30 mm, the mesh is selected with wire-to-projectile diameter ratios from 0.07 to 0.10, so that 4 to 6 wires are "cut" by the diameter of the projectile. In these studies, an MDB was tested with a mesh that would be effective against a spherical projectile with the same mass as the thin HVL flyer plate.

The MDB shields were also subjected to HVL testing. The mesh consisted of 0.3 mm diameter aluminum wires in a ~12 by 12 per cm^2 square pattern (the first series of tests used 0.58 mm diameter wires in a ~9 by 9 per cm^2 square pattern--see Christiansen, 1990). The second bumper was a continuous 0.635 mm-thick aluminum 6061-T6 sheet 51 mm behind the mesh. A third bumper consisted of a number of sheets of Kevlar® 710 mounted 203 mm away from the second bumper and 51 mm in front of the back sheet. The MDB's that were tested had Kevlar® bumpers consisting of between 4 and 6 layers. The 6061-T6 aluminum back sheets that were tested were 1.6 to 2.0 mm thick.

3. HYPERVELOCITY IMPACT EXPERIMENTS

At the lower end of expected debris impact velocities, the degree of damage to various shield configurations can be generally predicted quite well both with analytic methods (Cour-Palais, 1969; Wilkinson, 1969) and hydrodynamics code simulations (Hertel *et al.*, 1992). At impact velocities below about 7 km/s, these calculations have been validated with experiments performed on two-stage light gas guns. With the recent development at Sandia National Laboratories of a hypervelocity launch capability (Chhabildas *et al.*, 1992a, b) it has become possible to perform experiments over the velocity range of 7 to 12 km/s. This higher velocity regime has previously been inaccessible for gram-sized plates but is necessary to evaluate various debris shield configurations in the mass and velocity regime associated with the bulk of orbital debris.

3.1 The HyperVelocity Launcher (HVL)

Though the hypervelocity launcher at Sandia has been described elsewhere (Chhabildas *et al.*, 1992a,b) it will be summarized briefly here. There are theoretical as well as practical limits on velocities that can be attained by two-stage light gas guns (Charters, 1987). To launch flyers to hypervelocities (in the range of 7 to 12 km/s), higher loading pressures are required. These higher velocities are attained by a scheme in which a fraction of the momentum of a projectile launched from a two stage light-gas gun is transferred to a lighter, stationary flyer plate. A multi-step "shockless" loading is required (to accelerate the plate without melting or fragmenting it). This is accomplished by means of a graded-density layer that is carried by a projectile and impacts the flyer.

The diameters of the flyer plate assemblies used in this set of experiments varied from 17 to 19 mm. The flyer deforms somewhat as it is accelerated, so at impact its diameter and effective areal density may be different (see Fig. 3 and section 5). There is also a later arrival of debris associated with the launch of the flyer. This "launch debris" is made up of remnants of the graded-density impactor and the rest of the projectile, as well as portions of a guard ring and debris generated by its impact on a stripper. Because of this ancillary debris from the launch, there is a limited time frame during which useful data can be collected. The estimated time of arrival of the launch debris at the shield assembly marks the end of the time window for useful "real-time" data collection.

3.2 Diagnostics

Two primary methods of instrumentation were used to record data from these experiments: flash x-rays and fast framing photography. The x-rays were principally used to determine the velocity of the flyer and its condition just prior to impact on the shield assembly The framing cameras recorded the propagation and evolution of the debris clouds generated by the impact on the bumper shields, and monitored the condition of the back sheet. In a few cases, flash x-rays

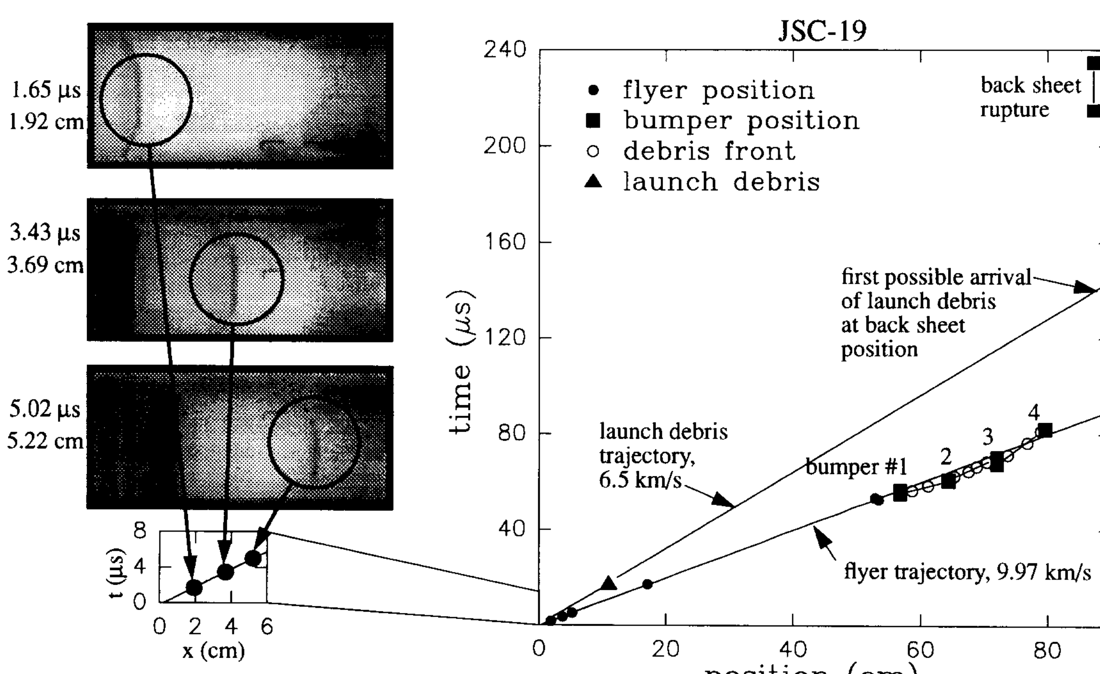

Fig. 2. X-ray images of flyer and x-t diagrams for JSC-19.

were also used to capture the shape and position of the debris cloud a few microseconds after impact of the flyer. Because of present space limitations, these images will be discussed in a subsequent report (Boslough *et al.*, 1993). Several flash x-rays were set to fire in sequence to capture the flyer at various positions along its flight path. The first three x-ray images of the launch sequence are depicted in Fig. 2 for experiment JSC-19. To determine the position of the flyer, the position of its x-ray image was measured relative to markers on a calibration rod that was placed along the boreline for calibration x-rays prior to the experiment. The flash time of each x-ray was recorded on a common time base with a LeCroy 8828 digitizer. To determine the flyer velocity, a data point corresponding to each x-ray image was plotted in the x-t plane, and a linear regression was performed. Such a plot is shown for experiment JSC-19 in Fig. 2. The origin of the plot is approximately at the time and position of projectile impact on the flyer. To determine the condition of the flyer at impact, it was imaged by means of flash x-ray radiography during its approach to the bumper. In Fig. 3(a), images of the flyer condition are reproduced for several selected experiments. In some experiments, the launch debris described in section 3.1 was imaged using flash x-rays, and its velocity was determined (Fig 2). By extrapolating its trajectory to the back sheet position, the time window for useful data collection can be estimated.

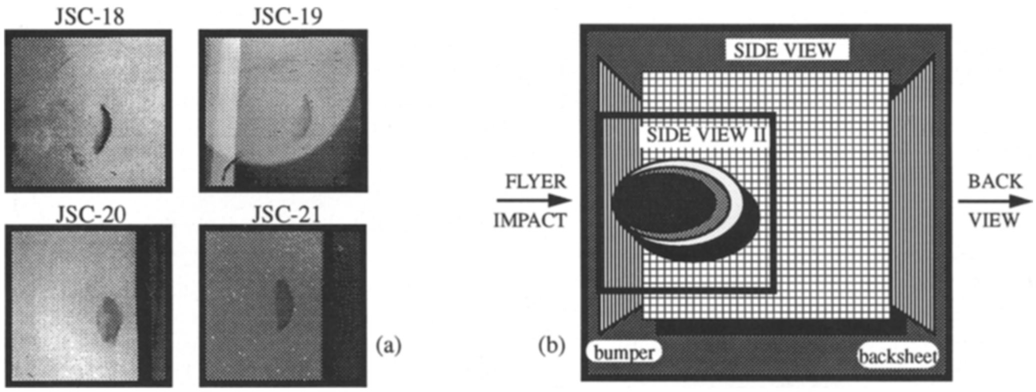

Fig. 3. (a) Flash x-ray photographs of flyers, (b) schematic of framing camera fields of view.

3.3 Framing Photography

In most of the experiments, two framing cameras viewed the shield assembly from the side. Because the framing camera images are emphasized in this paper, a schematic representation of the view from each camera is depicted in Fig. 3(b). In this example, the Whipple shield configuration is shown. The effect of perspective from the cameras is seen, and it is clear that the grid in the background cannot be used as a direct scale for position of the debris. The debris front is assumed to lie along an extension of the boreline of the gun, and is therefore closer to the cameras and has a different magnification factor. Calibration images were taken with a ruler on the boreline to determine the ratio of magnification factor on the boreline to that on the gridplane. Since the gridplane is visible in the shot images, it can be used with the measured ratio to determine the appropriate magnification factor. The schematic nature of Fig. 3(b) should be emphasized; the perspective is exaggerated, and in reality the two side cameras view the scene from different angles.

4. RESULTS AND DISCUSSION

Numerous experiments have been performed on the three different debris shield configurations; parameters that were varied included flyer material, mass, and velocity. Not all these experiments are discussed in detail here; instead several were chosen to highlight the effects of particular differences in either the experimental results or the impact configuration. In this section, the test results at impact velocities of about 7 and 10 km/s are summarized in detail for the selected experiments. The impact conditions are given in Table 1. Whenever a given test resulted in a rupture of the back sheet due to interaction with the debris generated by the impact of the flyer on the bumper, the test was classified as "fail". When the back sheet remained undisturbed, or was deformed without rupturing over the useful duration of the experiment, then it was classified as "pass". In a few tests we observed minor "pinhole" penetrations that did not continue to grow. These were classified as "threshold" tests.

4.1 Whipple Bumper Shield

4.1.1 Experiment JSC-3. This experiment examined the response of a Whipple bumper shield to the impact of a 0.781 g aluminum flyer at 7.10 km/s. The bumper thickness was 0.30 mm, which was chosen on the basis of calculated full melting of a 0.8 g, 19 mm diameter, 1 mm flat flyer impacting normal to the bumper surfaces. The back sheet thickness was 4.06 mm, and the distance between the two aluminum sheets was 305 mm. In Fig. 4, the side view framing sequence of images is shown. The times associated with each frame are relative to the estimated time of impact on the

Table 1. Summary of Experiments Performed on Debris Shields.

Shot No.	Shield type	Flyer Material	Initial Flyer Thickness (mm)	Initial Flyer Diameter (mm)	Initial Flyer Mass (g)	Impact Velocity (km/s)	Debris Shield Variable[a]	Back Sheet Thickness (mm)	Pass/Fail
JSC-3	WBS	Aluminum	1.02	19.3	0.781	7.08	0.305	4.06	Fail
JSC-5	WBS	Aluminum	1.04	19.3	0.793	7.19	1.27	4.06	Pass
JSC-9	WBS	Aluminum	1.03	19.0	0.777	9.52	0.305	4.06	Fail
JSC-12	WBS	Magnesium	1.01	19.0	0.503	9.92	1.27	4.06	Threshold
JSC-15	MSS	Aluminum	1.04	19.1	0.790	9.60	BF54	2.03	Pass
JSC-18	MSS	Aluminum	1.00	17.0	0.599	9.85	BF54	2.03	Pass
JSC-19	MSS	Aluminum	1.06	17.0	0.634	9.97	BF54	2.03	Pass
JSC-20	MSS	Aluminum	0.99	16.9	0.594	10.12	AF62	2.03	Pass
JSC-6	MDB	Aluminum	1.03	19.0	0.766	7.46	4	1.59	Threshold
PII-3	MDB	Aluminum	1.05	19.0	0.794	9.60	5	2.03	Pass

a. Bumper Thickness (mm) for WBS, Nextel® type for MSS, number of Kevlar® layers in third bumper for MDB

bumper. A rapidly expanding debris cloud can be seen propagating to the right from the point of impact. The front edge of the debris is well-defined, and the apex is lined up with the centerline of the experiment. A thin envelope of bright material appears to have separated from the darker, main mass of debris, and moved ahead at higher velocity. By measuring the position of the fronts of these debris clouds as a function of time, the velocity of the leading edge of each front can be determined by means of linear regression. This method assumes that no acceleration of the debris front takes place after impact. This assumption is valid within the precision of position measurements, and the velocity is about 5.5 km/s for the dark, main mass and 7.0 km/s for the brighter envelope. The debris velocities determined from framing images in this way are termed "photo-visual" velocities, to distinguish them from velocities determined via flash x-rays which were included in some experiments. The photo-visual velocities tend to be somewhat different than x-ray velocities because in the former method visible light that is reflected or radiated from x-ray-transparent matter can be measured. In the final (42 μs) frame, the debris cloud has already impacted on the back sheet, as indicated by the resulting flash. In Fig. 5, the side view (II) data are shown. Common features can be seen, but from a different angle. In Fig. 6(a), the back surface view framing sequence is shown. The framing interval is 5 μs, and the first frame time is 44.7 μs after bumper impact. It is clear that by this time the back sheet has already been deformed by the debris cloud that was seen impacting it a few microseconds earlier in the side view. In the following frames, a secondary debris cloud continues to grow, indicating that the back sheet has ruptured.

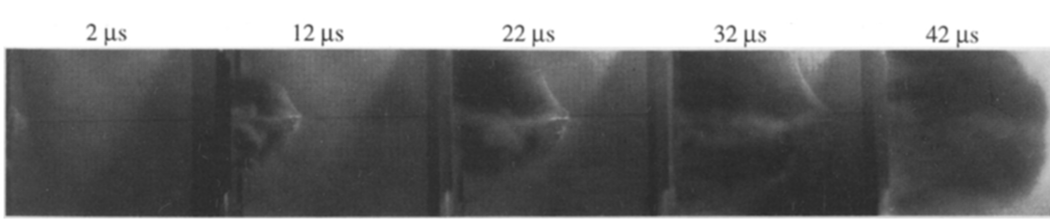

Fig. 4. JSC-3--Side View.

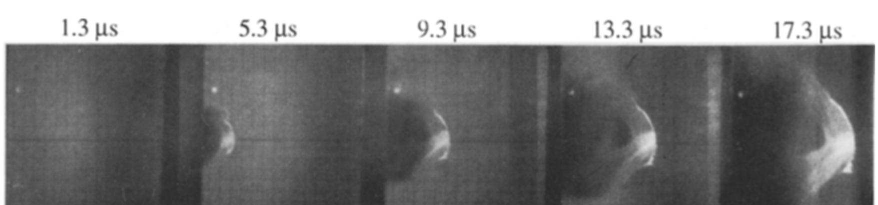

Fig. 5. JSC-3--Side View (II).

The information in these images can be conveniently presented as time vs. position in an "x-t" diagram, as shown in Fig. 6(b). In this diagram, δx is the distance behind the bumper, and δt is the time after estimated impact at the bumper. Symbols indicate time-position data as determined from the framing images. The solid line is the best-fitting debris front trajectory. The debris front velocity is the reciprocal of the slope of this line. For reference, the extension of the

(a)

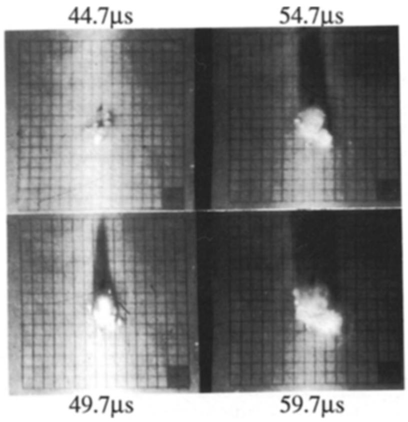

(b)

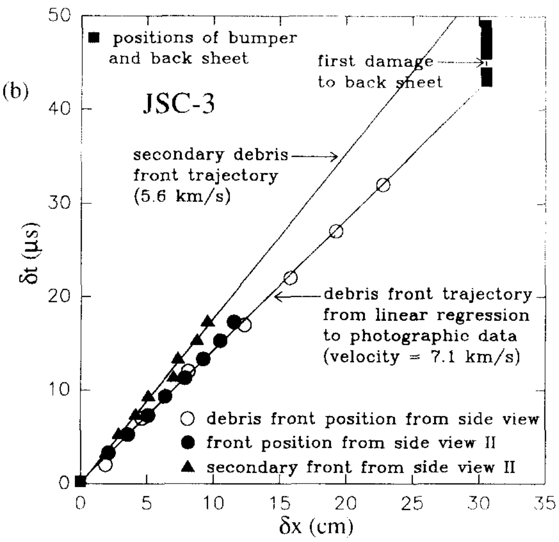

Fig. 6. (a) JSC-3--Back View,
(b) JSC-3--x-t diagram.

flyer velocity is also plotted (this would be the trajectory of the flyer in the absence of the shield). Because the back sheet clearly ruptured at an early time, JSC-3 was classified as a "fail" in Table 1.

4.1.2 Experiment JSC-5. Because flash x-ray images of flyers show that they tend to be tilted as well as bowed, their areal densities are higher than if they had remained flat. For this reason, a thicker bumper than that used in JSC-3 would be required to provide the same amount of irreversible shock energy per unit flyer mass, thereby completely melting the flyer. In JSC-5, the bumper thickness was increased to 1.27 mm. The debris structure and evolution was similar to that noted for JSC-3, with a separation into a dark mass and a brighter, faster envelope. Side and back views were shown by Ang *et al.* (1992), where the leading edge of the outer layer could be seen to impact the backsheet between 37.8 and 42.8 μs after bumper impact. The photo-visual velocity of this debris was about 6.8 km/s, and that of the dark mass was 5.6 km/s. The back surface view of the back sheet showed that some deformation had taken place by 57.4 μs, but 45 μs later the sheet was still intact. Because the back sheet remained intact up to 100 μs after bumper impact, JSC-5 was classified as a "pass".

4.1.3 Experiment JSC-9. For this test, we returned to the original Whipple bumper thickness of 0.30 mm, but the impact velocity was increased significantly to 9.52 km/s. The debris cloud developed very rapidly (see Ang *et al.*, 1992), with the outer, brighter cloud expanding more rapidly, at about 12 km/s. It remained roughly spherical, and was tenuous enough to be transparent. The inner, darker cloud expanded more slowly, at 9.7 km/s and retained a more prolate shape. It appeared to be more dense, as it obscured the view of the grid in the background. The structure of the debris was qualitatively different from that generated by lower velocity impacts, but the outer envelope seen in those experiments may be related to the outer cloud observed in this one. The most reasonable interpretation is that the outer cloud is vapor and small droplets of liquid condensing from it, while the inner cloud consists of dense, mostly liquid debris. The back view framing sequence indicated that the backsheet was not penetrated until δt=40.4 μs, after which damage proceeded very rapidly compared to shot JSC-3. This is 18 μs after the outer low density debris cloud arrived at the backsheet, and is consistent with the arrival of the dark, inner cloud. The results of test JSC-9 were clearly classified as "fail".

4.1.4 Experiment JSC-12. For JSC-12, the thick (1.27 mm) Whipple bumper was used with a high velocity (9.92 km/s) flyer. In this case, the flyer mass was reduced to 0.503 g, by using a magnesium plate. The side view sequence (Fig. 7) shows that, like JSC-9, there is a clear separation of the debris cloud into two distinct components. Also as with JSC-9, the perforation of the backsheet appears to take place significantly later than arrival of the faster cloud. The outer debris velocity for JSC-12 was determined to be over 15 km/s, and that of the inner cloud was about 10.6 km/s. Because there was no apparent growth of the hole after the plate was penetrated, JSC-12 was classified as "threshold".

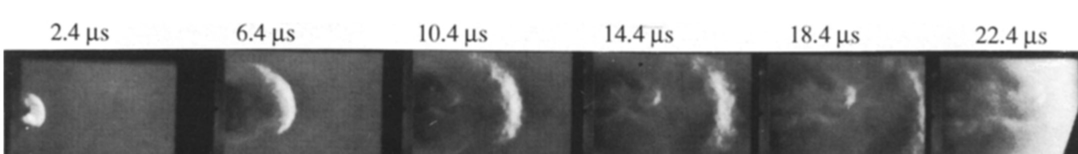

Fig. 7. JSC-12--side view (II).

4.2 Multi-Shock Shield

4.2.1 Experiment JSC-15. This was the first test involving the MSS configuration made up of the BF54 Nextel® fabric as described in section 2.2. The flyer was 0.790 g of aluminum, and it was launched to a velocity of 9.60 km/s. The final x-ray radiograph of the flyer before impact indicates that it consisted of a large piece with some small trailing fragments. The side view framing images shown in Fig. 8 indicate a somewhat different debris cloud development and evolution than was observed in the Whipple bumper experiments. Most noteworthy is the fact that the debris front velocity slows down with each subsequent shield interaction. For example, at δt=6.5 µs, the debris from impact on the first shield has just arrived at the second shield, as indicated by the brightly glowing area on the downrange side of the second shield. By 16.5 µs, debris has arrived at the third shield, but it is another 30 µs or so before the main mass of debris hits the fourth shield Another feature of note is the apparent generation of multiple debris fronts that behave differently upon interaction with the shield layers. In the 16.5 µs frame (when the debris is between shields 2 and 3), two distinct debris types can be seen which have much in common with those identified for shot JSC-9 and JSC-12. The behavior of the debris fronts when they arrive at the Nextel® shields supports the previous identification of the diffuse, faster front with vapor and mist, and the slower front with dense solid and liquid. The debris in the faster front appears to pass though the holes in the fabric with little interaction. This effect can most readily be seen in upper part of the 26.5 µs frame, where the faster front is approximately continuous across shield 3, whereas the bright, slower front shows a discontinuity. These phenomena are discussed further in section 4.2.5. In the back view sequence (not shown), the first indication of damage is not until about 146 µs, so JSC-15 is a "pass".

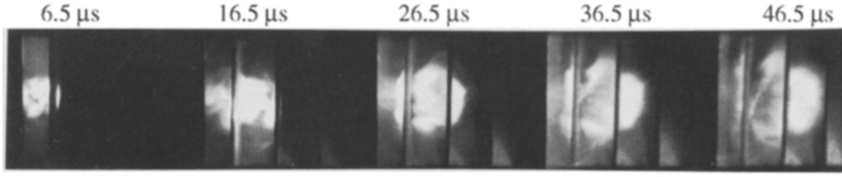

Fig. 8. JSC-15--side view.

4.2.2 Experiment JSC-18. The only difference between this test and JSC-15 was the lower flyer mass (0.599 g), the slightly higher impact velocity (9.85 km/s), and the condition of the flyer before impact (fully intact but bowed-see Fig. 3). The debris cloud images (Fig. 9) are qualitatively similar, but have a greater degree of axial symmetry, possibly due to the more symmetric condition of the flyer at impact. The discontinuity of the debris front on either side of each shield is more extreme (giving rise to a "wedding cake" like structure). In this case the diffuse, faster front also appears to be discontinuous. There is some evidence for a third component of debris; a roughly spherical bubble centered about a point moving downrange. One such bubble can be seen growing and moving downrange in the third intershield space between 23.6 and 38.6 µs. After 38.6 µs, a similar bubble evolves in the last intershield space; it is sharpest in the 43.6 µs image. The JSC-18 data were divided into four sets, each corresponding to front measurements within one of the four 76 mm-wide intershield spaces. Each set of data (some containing only two points) were independently fit to a straight line to estimate the velocity. The approximate velocities determined in this way were, in chronological order: 15, 9, 4, and 6 km/s. Because of the small data sets and the relatively large uncertainties these velocities are estimates, but the general trend indicates a decrease in velocity with each shield interaction. In this experiment, there was a long delay between the estimated time of arrival of debris upon the back sheet and the first sign of damage, so JSC-18 is a "pass"; the rupture was caused by the ancillary "launch" debris.

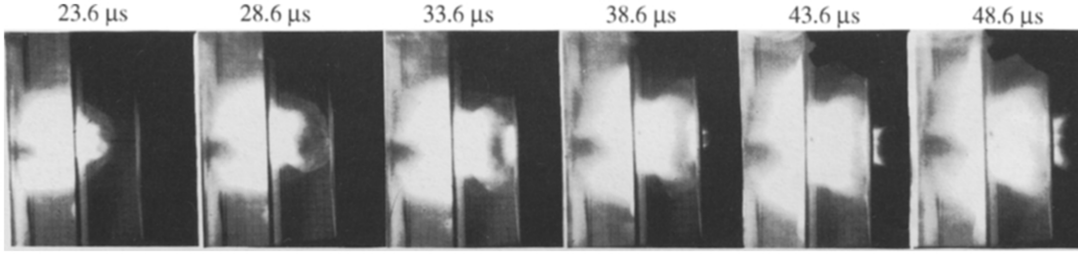

Fig. 9. JSC-18--side view (II).

4.2.3 Experiment JSC-19. The only substantive difference between this test and JSC-18 was in the choice of Nextel®. In this case it was BF54 "sized", *i.e.* heated with an anti-irritant coating so that it can be handled manually). The mass and velocity of the aluminum flyer were almost the same, at 0.634g and 9.97 km/s, respectively. The evolution and shape of the debris clouds are remarkably similar for both experiments (Fig. 10). The growth and motion of the debris bubble at 24.8 and 29.8 µs is particularly clear and sharp. Another feature can also be seen in the JSC-19 images. A uniformly-spaced pattern appears just aft of at the third shield (approximate center of field-of-view). The horizontal streaking of these features is consistent with debris streaming through a periodic pattern of holes in the woven fabric shield. Position-time histories are plotted in Fig. 2, with optimal linear fits indicating a decrease in debris velocity from 14 km/s behind the first shield to 5 km/s behind the third, in general agreement with JSC-18. Also plotted in Fig. 2 is the time of the last image of the back surface of the back sheet before the first indication of penetration.These images show no damage to the back sheet until about 180 μs after the flyer impacts on the first bumper, so JSC-19 is a "pass".

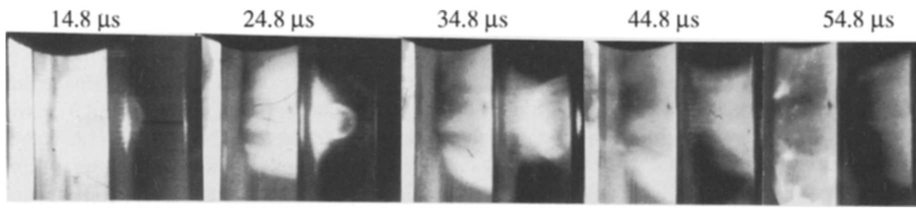

Fig. 10. JSC-19--side view (II).

4.2.4 Experiment JSC-20. This test was similar to the previous two, but made use of lighter-weight AF62 Nextel®. The aluminum flyer mass was 0.594 g, and the velocity was 10.12 km/s. The flyer was intact just before impact (Fig. 3), but it appears be quite irregular in shape compared to the previous two experiments. This irregularity is probably the reason for the somewhat less symmetric debris cloud form seen in the side view sequence (Fig. 11, 12a).However, the main features noted before are still present. Between 13.5 and 17.5 μs, a moving debris bubble can be seen in addition to an outer diffuse and inner, denser cloud. Further downrange, it can be seen that there is actually more than one diffuse debris cloud. This is most apparent at 40.6 μs in Fig. 12(a).

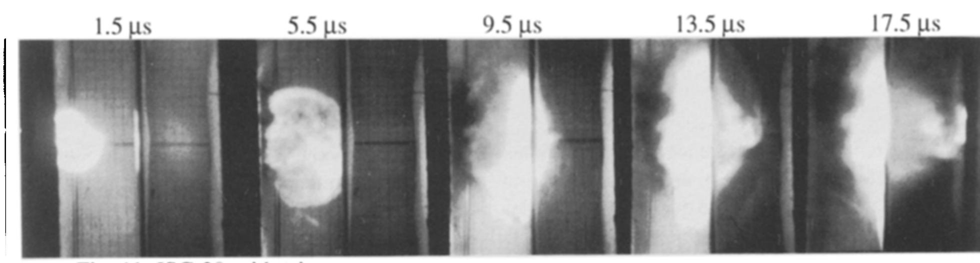

Fig. 11. JSC-20--side view.

For this experiment, an attempt was made to determine time-position data for all the debris fronts. These are plotted in Fig. 12(b), where different symbols are used to denote different debris fronts, and the calculated velocities correspond only to the fastest, outermost front. The back view of the back sheet shows that it is still fully intact as of 160 μs after impact on the first bumper, so this test was a "pass".

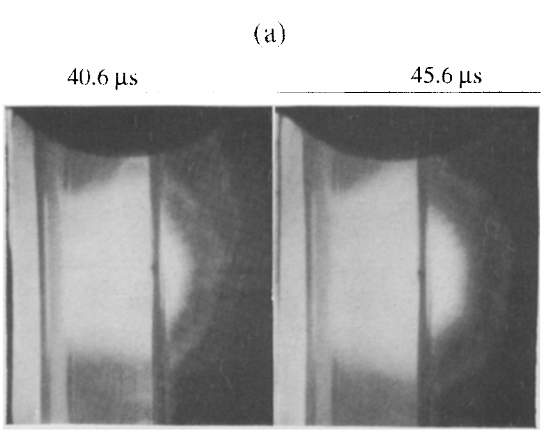

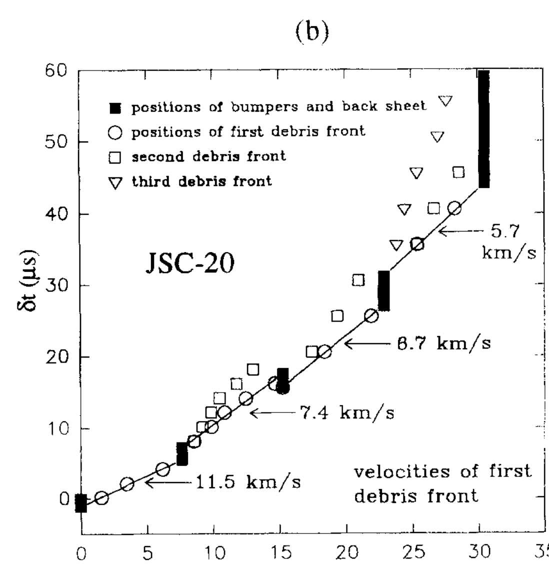

Fig. 12. (a) JSC-20--side view (II),
(b) JSC-20--x-t diagram.

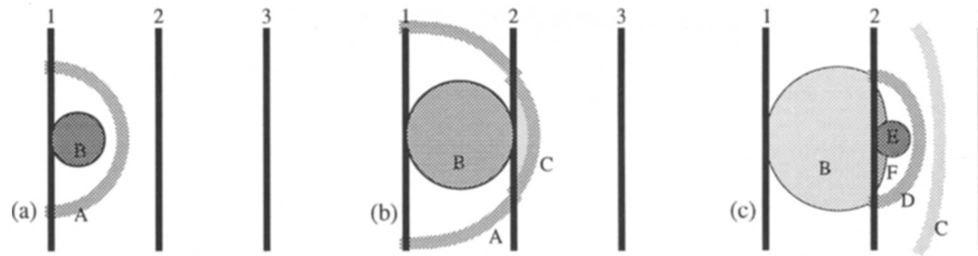

Fig. 13. Hypothetical evolution of MSS debris cloud.

4.2.5 Discussion of MSS Debris Evolution. The flyer impact and subsequent interaction between debris fronts and additional shield layers clearly leads to a richer, more complicated structure and evolution of debris for this shield assembly in comparison to that for the simple metallic WBS. Fig. 13 depicts a highly simplified interpretation of the origin of the various parts of the debris cloud. The figure shows a sequence of schematic snapshots of the development of an idealized debris cloud as it progresses through the first two shields. Figure 13(a) shows the structure of the debris shortly after impact at which time it has separated into two components: *A*, the vapor cloud, and *B*, the dense solid/liquid debris bubble. The situation shown in Fig. 13(b) is the instant the dense debris bubble arrives at the second shield. A portion of the vapor cloud *A* has already passed through the porous fabric, giving rise to vapor cloud *C* in the second space. Figure 13(c) depicts the situation after the main bubble *B* has collided with the second shield. The vapor cloud *C* has propagated downrange, and the mass concentration of flyer material at the apex of bubble *B* generates a pair of debris components, *D* and *E*, that are analogous to *A* and *B* from the original impact. Finally, the "skin" of bubble *B* interacts with the second shield, generating debris front *F*. Obviously, if a similar set of interactions takes place at each shield, the number of debris components will increase much more rapidly than the number observed in the framing images. However, this picture does provide a conceptual framework for identification of various debris fronts.

4.3 Mesh Double Bumper

4.3.1 Experiment JSC-6. In this test, an MDB shield such as that described in section 2.2 was subjected to impact by a 0.766 g aluminum flyer at 7.46 km/s. The flash x-ray image of the flyer before impact indicates that it was intact and bowed, but was tilted at impact. It is very difficult to see the form of the debris between the mesh and the second bumper in the framing sequence because of impact flash (Fig. 14), and it is not possible to make any quantitative statements about it. However, the debris cloud that forms immediately downrange from the second bumper has a very well-defined leading edge from which it was easy to determine a velocity of about 6.5 km/s. This debris cloud is quite different from that generated by the Whipple bumper, in that the outer envelope of faster material is not present.

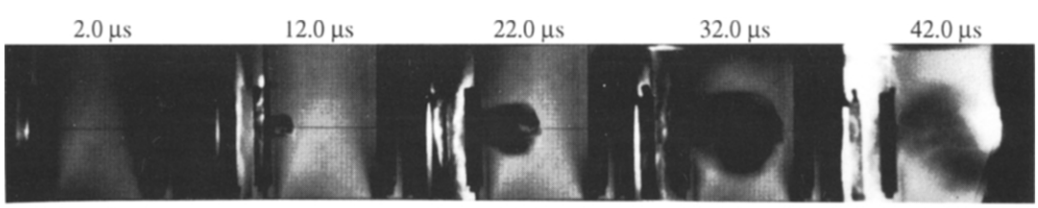

Fig. 14. JSC-6--side view.

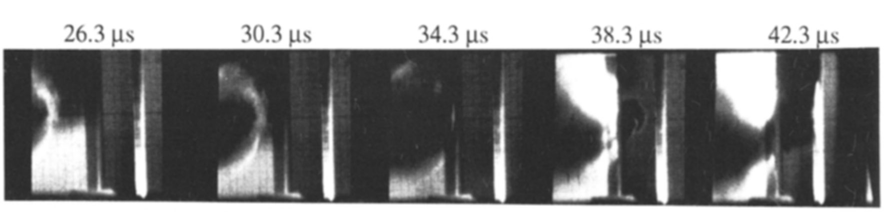

Fig. 15. JSC-6--side view (II).

This cloud can be seen colliding with the third (Kevlar®) bumper in Fig. 15, generating another debris cloud in the following space with a velocity of roughly 8 km/sec. This increase in velocity after interaction with a bumper was not observed in any of the MSS tests (within the uncertainty of measurement). However, there are valid reasons why metal debris impacting a polymer-containing composite could generate a secondary debris cloud with a higher expansion velocity as observed. The sequence of back surface images (not shown) demonstrate that the backsheet is perforated quite early by the debris, but the perforations do not appear to grow very much. For this reason, JSC 6 was classified as being on the threshold of failure.

4.3.2 Experiment PII-3. In this test, a 0.794 aluminum flyer hit an MDB at 9.6 km/s. A more massive MDB was used, with five layers of Kevlar in place of the four layers used in the previous experiments, and with the aluminum backsheet increased in thickness to 2.03 mm. The framing images in Fig. 16(a) show the debris approaching and impacting the second (solid aluminum) bumper, and the debris cloud that is generated from that impact. The velocity of the debris in the first intershield spacing was about 7.5 km/s. However, a faster, more tenuous front is also visible. The debris in the second spacing was moving at a remarkably high velocity of nearly 16 km/s. This increase in velocity at the second bumper for 10 km/s impacts has since been confirmed by other experiments on MDB's. The lower, post-Kevlar debris velocity of about 5 km/s is a lower bound. Because the backsheet did not suffer damage until well after arrival of ancillary launch debris, experiment PII-3 is listed as a "pass".

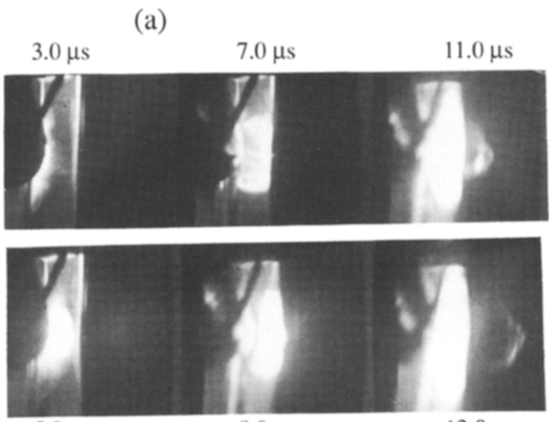

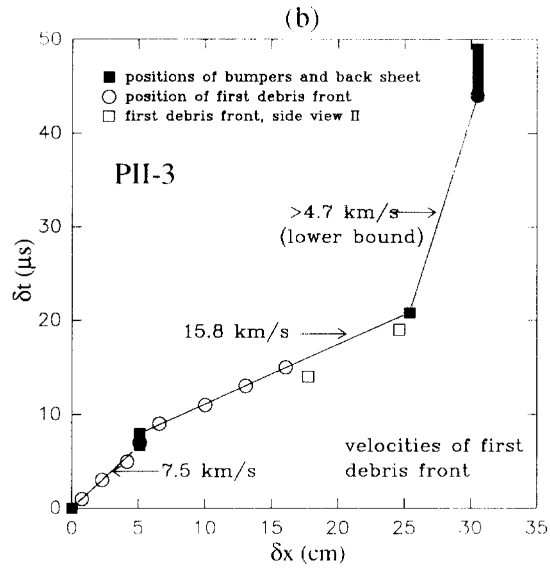

Fig. 16. (a) PII-3--side view.
(b) PII-3--x-t diagram.

5. ANALYSIS AND COMPARISON OF RESULTS

The analysis of the shielding concepts reported in this section is preliminary because the flyers are bowed in shape as opposed to the flat disks that have been considered analytically. In some experiments, the bowed disks are skewed or tilted as well (Fig. 3), so the initial impact is no longer an axially symmetric process. Irregular impacts are far more likely than geometrically simple impacts to occur in orbit, but they are more difficult to simulate with computer codes. Some modelling of the flyer and first bumper interaction is needed to understand the complex fragmentation that takes place. The purpose of the present test series was to extend the shield development undertaken with spherical aluminum flyers at 7 km/s (Cour-Palais *et al.*, 1992) to higher velocities. However, it is possible to glean some interesting results if we consider the relative areal densities of the intact flyers and the shields.

Radiographs of the flyers taken prior to impact (Fig. 3) show that the curvature of the disks reduces their effective diameter. Given a disk thickness of 1 mm and diameter of 19 mm, the mass of an aluminum flyer is 0.77 g and its areal density is about 0.27 g/cm^3. If the curvature decreases its diameter to a chord of 17 mm, the areal density increases to a mean of about 0.34 g/cm^3. The diameters of a number of flyers were measured from the x-ray images, and their known masses (Table 1) were used to determine the areal densities at impact (see Table 2). These numbers are based on the assumption that the single radiographic projection available is representative, *i.e.* that flyers are approximately symmetric. In a few of the experiments, orthogonal x-rays taken prior to impact show that the flyer is still approximately circular (for those experiments, the mean diameter is given). This interpretation is also supported by the symmetric and smooth appearance of most of the flyers in the radiographs. However, flyers may be tilted and their areal projection on the plane perpendicular to the velocity vector will not be circular, giving rise to significant uncertainty. The resulting flyer areal densities were used to calculate several shield parameters (Table 2) that can be compared directly with similar results obtained with undeformed spheres and disks launched by a light-gas gun to 7 km/s.

The WBS tests can be summarized as follows: JSC-3 failed, JSC-5 passed but the back sheet experienced two small dimples, JSC-9 failed and JSC-12 had one small perforation and was on the threshold of failure. Thus the ballistic limit for a total shield areal-density (A-D) of 1.44 g/cm^2 is an initial impact momentum between the 5.7 x 10^5 dyne-seconds for JSC-5 and 5.0x 10^5 dyne-seconds for JSC-12 (Table 2). However, in JSC-12, the flyer had a ring of fragments, so its effective A-D was lower. It is possible that a fragment escaped bumper impact and did further damage, or that there were more solid bumper fragments for the lower-momentum impact (JSC-12).

The four MSS tests (JSC-15,18, 19, and 20) all passed. The first thing to note is that the total shield A-D's are much lower than for the WBS shields. The total A-D is 31% less for the MSS tested in JSC-18 compared to the WBS in JSC-12, yet the MSS survived a higher-momentum impact than the WBS, which was on the threshold. A comparison of JSC-15 and JSC-19 with JSC-12 shows that the MSS also passes with a 31% lower A-D for a heavier, denser flyer. Finally, JSC-20 can be compared with JSC-18 to show that the total shield A-D can be further reduced to 33% lighter than the heavy WBS. The MSS shields tested in JSC-18 and 19 were slightly lighter than the "baseline" shields that were derived in previous tests (Cour-Palais *et al.*, 1992). In those tests a 1.27 g spherical aluminum projectile at 6.73 km/s was the ballistic limit for an impact momentum of 8.5 x 10^5 dyne seconds. The limited results of these tests suggest that a 10 km/s bowed disk projectile is more damaging than a spherical projectile for a given momentum and areal density, in agreement with Hertel *et al.*, 1992 who showed that for a "plate" impact (unlike a spherical impact) the resulting debris cloud tends to be more channelled and focussed. The corrections to allow for shape effects in the predictive equations derived from light-gas gun tests with spheres at 7 km/s must await the further tests that are planned at this facility.

The two MDB experiments were selected to show the effect of bumper areal density on survival of this design, and to compare their effectiveness to heavier WBS's. JSC-6 was of the lightest-weight design, and was just on the threshold of failure. It is noteworthy that the bumper/flyer A-D ratio was lower by a factor of 3, and the total shield A-D was about 43% less than the WBS tested in JSC-3, which clearly failed under similar impact conditions (the flyer was highly tilted for JSC-6, giving it a high average areal density). PII-3 was a test of an MDB design with an areal density of 0.94 g/cm^2, slightly less than the MSS's, and 35% lighter than the WBS that barely survived similar loading conditions in test JSC-12. The flyer was highly deformed with a small radius of curvature, giving it a relatively high A-D. Nevertheless, the shield survived an impact with the largest flyer momentum test, with a lower bumper/flyer A-D ratio than any of the MSS tests.

Table 2. Debris Shield Test Parameters.

Shot No.	Flyer momentum (10^5 dyne·sec)	Effective flyer diam. (mm)	Mean flyer A-D, m_f (g/cm^2)	Bumper A-D, m_b (g/cm^2)	Backsheet A-D, m_{bs} (g/cm^2)	Total Shield A-D, m_s (g/cm^2)	Bumper/flyer A-D Ratio, m_b/m_f	Shield/flyer A-D Ratio, m_s/m_f
JSC-3	5.53	18.9	0.28	0.085	1.101	1.18	0.31	4.3
JSC-5	5.70	16.9	0.35	0.343	1.101	1.44	0.97	4.1
JSC-9	7.40	16.7^a	0.36	0.085	1.101	1.18	0.24	3.3
JSC-12	4.99	20.2^b	0.16	0.343	1.101	1.44	2.18	9.2
JSC-15	7.58	14.9	0.45	0.432	0.551	0.98	0.95	2.2
JSC-18	5.90	16.5	0.28	0.432	0.551	0.98	1.54	3.5
JSC-19	6.32	15.8	0.32	0.432	0.551	0.98	1.34	3.0
JSC-20	6.01	16.0	0.30	0.400	0.551	0.95	1.36	3.2
JSC-6	5.71	13.5	0.54	0.350	0.322	0.67	0.65	1.3
PII-3	7.62	14.3	0.49	0.382	0.555	0.94	0.77	1.9

a. Flyer is broken and has trailing fragments.
b. Includes diameter of fragment ring.

6. SUMMARY

Experiments have been performed on the Sandia's Hypervelocity Launcher to characterize and evaluate both simple and advanced shielding concepts that are proposed for use with spacecraft in low earth orbit, such as Space Station Freedom. Experiments were conducted over a velocity range of 7 to 10 km/s, a range heretofore not accessible by conventional smooth bore launchers. Orbital debris impact is simulated by launching a plate-like projectile at the proposed shield designs. The simple shield concepts make use of an aluminum Whipple Bumper Shield placed at a distance from its protective structure. Concepts for advanced shielding include both the Mesh Double Bumper and Multi-Shock Shields. Results and conclusions from these experiments may be summarized as follows:

Whipple Bumper Shield:

- A WBS whose bumper thickness is 0.3 mm is not sufficient to protect a back wall about 4 mm thick placed 305 mm away when an 0.78 g plate in the shape of a bowed disk initially about 19 mm in diameter by about 1 mm thick impacts it over a velocity range of 7 to 10 km/s.

- A similar WBS whose bumper thickness is increased to 1.3 mm is sufficient to protect a back wall about 4 mm thick placed 305 mm away under similar loading conditions at about 7 km/s, even when the total shield-to-projectile A-D ratio is slightly lower.

Multi-Shock Shield:
- The MSS is effective at dispersing incoming bowed disk flyers with masses up to 0.79 g (about 19 mm diameter by 1 mm thick) at velocities up to about 10 km/s. It consistently prevents rupture of a 2 mm thick back sheet located 305 mm from the front bumper shield.
- With an areal density reduction of up to 33%, the MSS is more effective than the WBS against impact by bowed disk aluminum plates at up to 10 km/s.
- The MSS disperses debris in both space and time, generating multiple debris fronts at each successive bumper. As the debris fronts propagate through the shield assembly, they slow down.

Mesh Double Bumper:
- An MDB with a back sheet 0.16 mm thick placed 305 mm from the first mesh location appears to be on the survival threshold when impacted by a 0.75 g bowed disk about 19 mm in diameter and 1 mm thick. This shield was about 43% lighter than a WBS that clearly ruptured under less severe impact conditions.
- With an areal density reduction of up to 35%, the MDB is more effective than the WBS against impact by bowed disk aluminum plates at up to 10 km/s.

General:
- A comparison of x-ray measurements and photographic measurements of the debris cloud suggest that the fastest photovisual debris is very low density.
- For normal impacts, bowed-plate or flat-plate projectiles are more damaging than spherical projectiles for a given momentum and areal density.

7. ACKNOWLEDGMENTS

This work was performed at Sandia National Laboratories, supported by the U.S. Department of Energy under contract DE AC04-76DP00789. We thank NASA for their interest and support. Brian Abeyta participated as a summer student by helping determine debris velocities from framing camera images.

REFERENCES

Ang, J. A., L. C. Chhabildas, B. G. Cour-Palais, E. C. Christiansen and J. L. Crews (1992). Evaluation of Whipple Bumper Shields at 7 and 10 km/s. In: *Space Programs and Technologies Conference*, AIAA Paper #92-1590.

Boslough, M. B., L. C. Chhabildas, R. D. Reinhart and C. A. Hall (1993). Hypervelocity Testing of Debris Shields against Impacts to 10 km/s. *Sandia Report*, in preparation.

Charters, A. C. (1987). Development of the High-Velocity Gas-Dynamics Gun. *Int. J.of Impact Engng.*, 5, 181-203.

Chhabildas, L. C., L. M. Barker, J. R. Asay, T. G. Trucano, G. I. Kerley and J. E. Dunn (1992a). Launch Capabilities to over 10 km/s. In: *Shock Waves in Condensed Matter--1991* (S. C. Schmidt *et al.*, eds.), pp. 1025-1031. Elsevier Science Publishers, B.V., Amsterdam.

Chhabildas, L. C., J. E. Dunn, W. D. Reinhart and J.M. Miller. (1992b) An Impact Technique to Accelerate Flier Plates to Over 12 km/s. *Int. J.of Impact Engng.*, this volume.

Chhabildas, L. C., E. S. Hertel and S. A. Hill, (1992c) Whipple Bumper Shield Tests at over 10 km/s. In: *Shock Waves in Condensed Matter--1991*, (S. C. Schmidt *et al.*, eds.), pp. 991-994. Elsevier Science Publishers, B.V., Amsterdam.

Christiansen, E. L. (1990) Advanced Meteoroid and Debris Shielding Concepts" In: *Procs. Orbital Debris Conf.*, AIAA Paper #90-1336.

Cour-Palais, B. G. (1969) Meteoroid Protection by Multi-Wall Structures. AIAA Paper No. 69-372.

Cour-Palais, B. G. and J. L. Crews, (1990) A Multi-Shock Concept for Spacecraft Shielding. *Int. J. Impact Engng.*, 10, 135-146.

Cour-Palais, B. G., A. J. Piekutowski, K. V. Dahl, and K. L. Poormon (1992) Analysis of the UDRI Tests on Nextel Multi-Shock Shields. *Int. J.of Impact Engng.*, this volume.

Hertel, E. S., L. C. Chhabildas, and S. A. Hill, (1992) Whipple Bumper Shield Simulations. In: *Shock Waves in Condensed Matter--1991*, (S. C. Schmidt *et al.*, eds.), pp. 987-990. Elsevier Science Publishers, B.V., Amsterdam.

Interagency Group (Space), (1989) Report for National Security Council, Washington, D.C.

Kessler, D. J., R. C. Reynolds, and P. D. Anz-Meador, (1989) Orbital Debris Environment for Spacecraft Designed to Operate in Low Earth Orbit. NASA TM 100-471.

Whipple, F. L. (1947) Meteorites and Space Travel. *Astronomical J.* 52, 131.

Wilkinson J. P. D. (1969) A Penetration Criterion for Double-Walled Structures Subject to Meteoroid Impact, *AIAA J.* 7, 1937-1943.